



Published in final edited form as:

J Phys Chem Lett. 2023 January 12; 14(1): 41–48. doi:10.1021/acs.jpcllett.2c03018.

X-ray Emission Spectroscopy of Single Protein Crystals Yields Insights into Heme Enzyme Intermediates

Sahand Emamian¹, Kendra A. Ireland^{†,2}, Vatsal Purohit^{†,2}, Kirklin L. McWhorter², Olga Maximova³, Winter Allen³, Scott Jensen³, Diego M. Casa⁴, Yulia Pushkar^{3,*}, Katherine M. Davis^{2,*}

¹Department of Physics, Emory University, Atlanta, GA 30322, USA

²Department of Chemistry, Emory University, Atlanta, GA 30322, USA

³Department of Physics and Astronomy, Purdue University, West Lafayette, IN 47907, USA

⁴Advanced Photon Source, Argonne National Laboratory, Lemont, IL 60439, USA

Abstract

Enzyme reactivity is often enhanced by changes in oxidation state, spin state, and metal-ligand covalency of associated metallocofactors. The development of spectroscopic methods for studying these processes coincidentally with structural rearrangements is essential for elucidating metalloenzyme mechanisms. Herein, we demonstrate the feasibility of collecting X-ray emission spectra of metalloenzyme crystals at a 3rd generation synchrotron source. In particular, we report the development of a von Hamos spectrometer for the collection of Fe K β emission optimized for analysis of dilute biological samples. We further showcase its application in crystals of the immunosuppressive heme-dependent enzyme indoleamine 2,3-dioxygenase. Spectra from protein crystals in different states were compared with relevant reference compounds. Complementary density functional calculations assessing covalency support our spectroscopic analysis and identify active site conformations that correlate to high- and low-spin states. These experiments validate the suitability of an X-ray emission approach for determining spin states of previously uncharacterized metalloenzyme reaction intermediates.

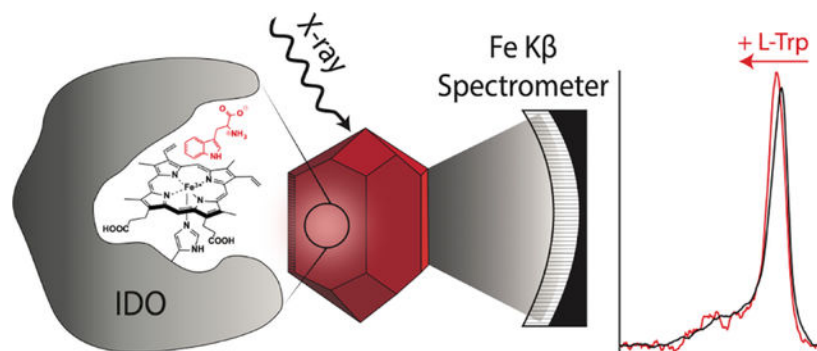
Graphical Abstract

*Corresponding Author: correspondence to: katherine.davis@emory.edu; ypushkar@purdue.edu.

[†]These authors contributed equally.

Supporting Information. The following files are available free of charge. Materials and methods, Figures S1–S4, Tables S1–S15. (PDF)

The authors declare no competing financial interests.



Keywords

metalloenzyme; spin; covalency; indoleamine 2,3-dioxygenase; iron; density functional theory; von Hamos

Metals are crucial to the biological processes of living organisms ranging from metabolism to transcriptional regulation and are incorporated into more than 40–50% of the proteome.¹ Enzymes, in particular, catalyze challenging chemical reactions by utilizing transition metal ions whose oxidation and spin states are coordinated with changes in atomic structure. While crystallographic studies are useful in determining the structural basis for enzyme reactivity, even time-resolved diffraction is insufficient for the characterization of metalloenzyme mechanisms as it provides little insight into the concerted redox changes that accompany catalysis. Complementary spectroscopic data is therefore essential. Moreover, electronic structure of the metal center must be monitored *in crystallo* for comparison to structural dynamics, as the kinetics may differ from those in solution.^{2,3} Among spectroscopies compatible with crystallography, inner-shell X-ray spectroscopies are unique as they are directly sensitive to the local electronic structure of the transition metal.^{4–6} This feature enables characterization of mechanistic intermediates without any *a priori* knowledge. X-ray emission spectroscopy (XES), in particular, is also adaptable for downstream time-resolved studies as it can be collected in an energy dispersive manner, meaning a statistical representation of the full spectrum is obtained irrespective of the collection time.⁷ Furthermore, unlike other techniques implemented online, such as UV-vis and Raman spectroscopies that are highly dependent on sample orientation, XES is compatible with serial crystallography approaches in which randomly oriented crystals are sequentially introduced to the incident X-ray beam.

Promising preliminary studies combining the techniques have been attempted at hard X-ray free electron laser (XFEL) sources, but limited availability of these facilities combined with their ill-defined modes of radiation damage have hampered broad application.^{8–10} To date, no transformative results have emerged, and the ability to evade X-ray-induced damage to sensitive metallocofactors is hotly debated. Fransson *et al.* describe the radiation-induced spectral effects on the Mn-containing metalloenzyme complex photosystem II as minimal up to flux densities of $\sim 10^{11}$ photons/pulse with the beam focused to $\sim 10 \mu\text{m}$, conditions common to fs XFEL pulses.¹¹ However, Jensen *et al.* report more significant spectral changes that would interfere with data analysis and defeat the purpose of tandem

spectroscopic measurements under similar conditions.¹² The source of these changes was ascribed to a multi-photon absorption process at the metal ions which cannot be avoided by sample dilution or alterations to the metal ion environment. By contrast, other groups argue the prevalence of an alternative mechanism where solvated electrons generated in the process of X-ray absorption by atoms surrounding the metal ion can be as impactful in causing changes to metal electronic structure on an ultra-fast time scale.¹³ It should be noted that the magnitude of spectral shifts can vary wildly depending on the element being probed and the average change in spin state, making any observable radiation-induced changes potentially problematic. To extend the application of XES to the broader enzymology community, this approach must become both more robust and more accessible. Synchrotron sources provide an ideal opportunity to achieve these goals as damage mechanisms are better characterized and experimental time more readily available.^{14–17} Furthermore, most metalloenzyme kinetics do not require femtosecond resolution.^{18–20}

Herein, we not only demonstrate the feasibility of collecting relevant XE spectra of metalloenzyme crystals using 3rd generation synchrotron sources, but further obtain insights into the heme-dependent human enzyme indoleamine 2,3-dioxygenase (IDO). IDO is a crucial component to metabolism of the amino acid L-tryptophan (L-Trp), catalyzing its conversion to N-formylkynurenine (NFK, Fig. 1A).²¹ Together, L-Trp consumption and NFK production contribute to suppression of the immune system through multiple biochemical pathways, making IDO a key drug target in the treatment of disease, most notably cancer.^{22–24} Despite its importance, a complete understanding of the mechanism remains elusive. The subtleties of even some stable intermediates, such as the reactant complex, have yet to be decoded. Particular ambiguity surrounds intermediate spin states and their origin, as mechanistic changes are characterized by a mixture of spin states that can be difficult to elucidate with less sensitive spin detection methods. Herein, we demonstrate that XES can be added as an informative tool to analyze this particular Fe-dependent enzymatic pathway, as well as other similar systems relevant for human health.

To both demonstrate broad applicability of the approach and observe electronic changes associated with the mechanistic behavior of IDO, we fabricated a new, wavelength-dispersive von Hamos spectrometer having an energy resolution of approximately 0.2 eV (see SI, Materials and Methods). Customizable design principles described previously were extended to develop the portable spectrometer in which three finely diced lithium niobate (LiNbO₃) analyzer crystals, arranged along a cylindrical curve, reflect emitted photons from 7012–7120 eV onto the surface of a pixel array detector (Fig. 1B).²⁵ This energy range encompasses Fe K β fluorescence, for which the most intense spectral lines correspond to photon emission from 3*p* to 1*s* transitions following excitation of an electron from the innermost shell, as well as the valence-to-core region corresponding to ligand orbital to 1*s* transitions not discussed in this report. In first row transition metals, coupling between the resultant unpaired 3*p* electron and the valence shell splits the main K β peak in two (K $\beta_{1,3}$ and the weaker satellite, K β'), thereby generating a powerful sensitivity to spin and, to a lesser extent, effective nuclear charge (Fig. 1C). More precisely, the greater the number of unpaired 3*d* electrons, the more substantial the 3*p*-3*d* exchange interaction.^{26, 27}

The spectrometer was commissioned at Sectors 14 and 20 of the Advanced Photon Source at Argonne National Laboratory. To assess its performance, we collected XE spectra for seven, primarily mononuclear Fe, model compounds (Fig. 2). In addition to visual inspection, quantification of changes in peak position were analyzed through comparison of first moments (i.e. intensity-weighted average emission energies, Table 1). Early XES experiments demonstrated that distinguishing between oxidation states of Fe via K β mainline analysis is particularly challenging.^{28, 29} Despite an increase in the number of unpaired *d* electrons in ferric complexes, associated increases in metal-ligand covalency often obscure expected changes to the magnitude of peak splitting.^{29, 30}

While differences between spectra of ferrous and ferric complexes having similar spin states are small, they are clearly detectable with our setup. Low-spin (LS) and intermediate-spin (IS) compounds follow expected trends in which the increasing spin state upon oxidation results in greater splitting and a shift of K $\beta_{1,3}$ to higher energies (Table 1, Fig. 2). Spectra of the selected high-spin (HS) compounds, by contrast, depict a decrease in splitting upon oxidation. This effect can be rationalized by the increased covalency of ferric oxide compared to ferrous sulfate heptahydrate due to the presence of comparatively stronger field ligands (O²⁻ versus water). The degree of covalency and Fe *d*-orbital spin density (Table 1) can be further simulated with quasi-restricted orbitals (QROs)^{31, 32} developed from density functional theory (DFT). More specifically, we calculate the degree of *d*-orbital character, which is simply a measure of the deviation of the molecular orbital (L \ddot{u} wdin) population from that of a free ion. Its complement (100 – *d*-orbital character) is therefore also a measure of covalency, as the ligand reduces the electronic population of the orbitals.³² It is important to note, however, that this approach to evaluating covalency was developed for application to octahedral and tetrahedral complexes and may not be as reliable for disparate geometries, such as five-coordinate ferrous IDO. From our QRO analysis, ferric oxide has more significant covalent interactions with its ligands, indicated by an 11.4% reduction in *d*-orbital character compared to ferrous sulfate heptahydrate. This enhanced hybridization of the Fe 3*d* orbital lowers the spin polarization density of the complex, redistributing K β' intensity and negating the effects of increased spin.

Spectral shifts associated with changing spin state are more significant, ranging from 1–2 eV (Table 1), in agreement with other studies, and are accompanied by a concomitant reduction in K β' peak intensity for LS Fe (Fig. 2).^{33, 34} To establish a more systematic and quantitative correlation between changes in spin state and peak position, we calculated integrated absolute differences (IADs) with respect to the spectrum of ferrocyanide. IADs have been demonstrated to vary linearly with spin, and a reference curve was generated using a subset of the complexes for which nominal spin states are well-characterized (see Figure S1, and see SI for methods).³⁵ With our choice of reference spectrum, a greater experimentally-determined IAD correlates to a greater spin state.²⁸

This type of analysis is particularly relevant for the study of species with unknown and/or complex spin states, such as those inherent to metalloenzyme intermediates. For example, calculated IAD values can be used to predict the spin of our selected Fe phthalocyanine samples. Intriguingly, the most accurate prediction is obtained for ferric phthalocyanine chloride (*S* = 1.75), which has been determined from magnetic susceptibility studies to

be an admixture of IS and HS species ($S = 1.85$).^{36, 37} The IAD-derived spin of ferrous phthalocyanine, by contrast, is 1.25, 25% greater than that measured experimentally.^{38, 39} It is unclear whether this discrepancy originates in the applied analysis or as-of-yet undetected subtleties of the ferrous phthalocyanine IS complex. Nonetheless, with an average deviation from known spins of approximately 15%, we were confident in our approach.

We therefore began working with single crystals of IDO. Data collection was attempted with both ‘continuous’ monochromatic and pulsed pink beam sources to assess the feasibility of future time-resolved measurements (see the SI for details). Due to time constraints associated with obtaining sufficient signal to differentiate the small shifts associated with changes in the effective nuclear charge, we opted to focus on elucidating spin states. The corresponding spectral changes are not only more significant, making them easier to detect, but spin states are also dominated by ligand field effects. As the Fe-coordination environment changes more slowly as a function of X-ray dose, this characteristic of metalloenzyme complexes should be less sensitive to X-ray-induced damage. XE spectra were collected for ferric and ferrous IDO as well as ferric IDO in the presence of its substrate L-Trp.

Not only is our spectrometer capable of attaining sufficient signal-to-noise to visualize the K β mainlines of IDO crystals following excitation, but we further observe a shift in the K $\beta_{1,3}$ first moment of approximately -0.58 eV upon complexation of ferric IDO with L-Trp (Fig. 3). Such a redshift suggests a decrease in spin state and positions the associated K $\beta_{1,3}$ peak closer to the LS ferrocyanide standard. By contrast, the K $\beta_{1,3}$ peak of ferrous IDO all but overlays with the spectrum of ferric IDO (Fig. 3). First moment analysis yields a shift of only $+0.12$ eV, placing both spectra directly adjacent to the HS standard. From a redox perspective, alignment of the ferrous and ferric complexes is not particularly surprising given that the X-ray dosage applied to these samples (see Table S1) has been shown to reduce ferric heme in other proteins,¹⁷ and spectral shifts due to changes in effective nuclear charge are small.³⁰ However, the cryogenic conditions of the experiment would likely prevent any large-scale structural changes that could dramatically affect the Fe-coordination environment and thus its respective spin states. This has been demonstrated previously through low temperature crystallographic characterization of ferrous and ferric IDO.⁴⁰ Altogether, observed changes in spectral position are consistent with previous experimental spin state analysis. And, to the best of our knowledge,¹⁰ the associated XE spectra of ferric IDO are the first to differentiate between spin states of metalloenzyme crystals having the same formal oxidation state.

Ferric IDO is known to be a pH-dependent mixture of HS ($S = 5/2$) and LS ($S = 1/2$) heme, and previous studies have estimated the ratio of HS to LS species to be roughly equal at pH 6.6.^{41, 42} Prior to structural characterization of the enzyme,⁴³ the identities of these HS and LS components were hypothesized to be histidine/water (Fig. 4A) and bisnitrogenous coordinated heme, respectively.⁴² Given the lack of a suitable distal histidine ligand, however, we propose that $3p$ - $3d$ exchange is instead mitigated by altered positioning of an active site loop (Fig. 4B, chains A & C from PDB ID 6E44), which promotes heme coordination by the carbonyl group of a constituent alanine and results in the observed LS contribution (Ala264).⁴⁰ Upon addition of substrate, the spin state equilibrium shifts toward

greater LS character, theorized to correspond to hydroxide-bound heme that is hydrogen-bonded to the pyrrolic nitrogen of L-Trp (Fig. 4C).⁴⁴ This ligand-dependent spin crossover is supported further by previous XES studies on metal-organic frameworks.⁴⁵ Papadopoulou *et al.* estimated a ligand distribution of approximately 33/7/60 (X/water/hydroxide) in the presence of L-Trp at pH 8, where X represents an active site residue, such as Ala264.⁴² Persistence of alanine coordination, and the associated steric constraints on the distal face of the heme cofactor, may help to explain ferric IDO's relatively low affinity for L-Trp.⁴⁰

To more rigorously assess the origin of associated LS components, we performed DFT optimizations and QRO spin analysis on truncated models of the IDO active site generated from published crystallographic models (Tables S10–S15).⁴⁰ In the absence of substrate, models depicting coordination by Ala264 (Table S14) returned the lowest energy values when heme was in a LS state (Table S15). Similar behavior was observed upon *in silico* addition of a hydroxide ion in the presence of L-Trp (Tables S11 & S15). Moreover, absence of the coordinating hydroxide ion led to a staggering 62.6 kcal/mol increase in the calculated energy of the substrate-bound complex. Together, these results stand in support of both hypotheses described above: (1) introduction of LS character in the absence of substrate occurs due to coordination by an active site alanine, and (2) upon L-Trp binding to the HS form of the ferric enzyme, associated deprotonation of the coordinating water lends additional LS character to the bulk sample.

Our ferric IDO crystals were generated at pH ~6.5 (see the SI), and thus, based on the heme populations observed by Papadopoulou *et al.* at this pH,⁴¹ we expect an approximately 50/50 ratio of HS/LS heme in the absence of substrate. This mixture of spin states is qualitatively reflected by the intensity of the observed $K\beta'$ peak, which is weaker than is typical for purely HS complexes. Despite accounting for the presence of substantial LS character in our ferric IDO samples, however, the spectral shift upon addition of substrate remains quite modest in comparison to spin state related shifts reported for Fe standards. Based on the position of the relevant $K\beta_{1,3}$ peak, it seems likely that our ferric IDO crystals co-crystallized in the presence of L-Trp contain significant HS contamination relative to the Papadopoulou *et al.* study of ferric IDO with L-Trp bound performed at pH 8. This result is not unexpected, as lower pH also enhances the HS character for ferric IDO without L-Trp present. Conveniently, we can estimate the relative HS and LS populations to a first order approximation, through application of the Henderson-Hasselbach equation, with the HS population corresponding to the water-bound state and the LS populations corresponding to the hydroxide-bound and Ala264-coordinated states. Through this approach, we estimate a modified ligand distribution of approximately 38/38/24 (Ala264/water/hydroxide) for samples generated at pH 6.5, assuming the 1:1 ratio of water-to-alanine ligation is maintained in the presence of substrate (see the SI). This first-order analysis explains the significant HS contamination of ferric IDO in the presence of L-Trp observed at this pH. Excitingly, we can closely reproduce these experimentally estimated spin state distributions via our IAD reference curve.

Calculated IAD values correlate to spins of 1.73 and 1.30 for ferric IDO and ferric IDO with L-Trp present, respectively (Fig. 5A, Table 1), suggesting an approximate error of 9%. Similar correlations can be made between the *d*-orbital character of the metallocofactor and

the splitting of the IDO mainline peaks (see the SI). This covalency analysis depicts trends that match ones obtained using IADs (Fig. 5B, Table 1). Ferrous and ferric IDO samples had very similar IAD-calculated spin states, which conform well to their independently calculated covalencies (23% and 24%, respectively). Conversely, ferric IDO with L-Trp present has lower nominal and calculated spin states, which correspond to the high calculated covalency (35%).

Analysis of the ferrous IDO spin state can be approached in a similar way, beginning with visual comparison of the IDO and ferrous sulfate $K\beta_{1,3}$ peak positions. This qualitative analysis would appear to suggest substantial HS character in crystals of the ferrous enzyme, in agreement with earlier room temperature resonance Raman, MCD, and UV-vis absorbance studies that observed spectral features consistent with a five-coordinate HS heme cofactor.^{41, 44, 46} X-ray crystallographic models depicting the ferrous enzyme further support this proposal, as the loop containing Ala264 does not directly interact with the metal ion, and no alternative distal ligand is identified (Fig. 4D).^{40, 47, 48} However, the intensity and shape of the ferrous IDO $K\beta'$ peak is more consistent with an IS or LS complex. We hypothesize that LS character may be introduced, at least in part, due to the cryogenic conditions (100 K) under which these data were collected, as has been inexplicably observed for other water/histidine-coordinated heme complexes.^{42, 49} Such behavior can likewise be employed to rationalize overlap with the ferric IDO spectrum, suggesting an upper bound of 25% LS contamination. Our IAD-predicted spin ($S = 1.77$) for the ferrous form of the enzyme further validates this hypothesis and correlates to ~89% HS character (Fig. 5A). The calculated covalency values also corroborate these findings: ferric IDO bound to L-Trp has the highest covalency, which depresses the spin state below those of ferrous and ferric IDO. While the integer spin states of ferrous complexes are difficult to confirm directly, our XE spectra provide clear evidence in support of a predominantly HS assignment, even at low temperatures.

In conclusion, the studies presented herein serve as a proof-of-concept for the collection of XE data of metalloenzyme crystals at 3rd generation synchrotron sources. Our analysis not only confirms that XES provide novel insights into complex metalloenzyme spin state equilibria, but further that this analysis can tolerate a degree of radiation-induced damage. Paired with time-resolved techniques, this methodology lends itself well to tracking intermediates of enzyme turnover, which typically include spin and oxidation state changes. With many facilities upgrading to 4th generation capabilities, the feasibility of these and future time-resolved X-ray emission experiments at synchrotron sources can only improve as dose deposition rates increase and enhance our ability to outrun radiolytic damage.^{14, 50–52}

Supplementary Material

Refer to Web version on PubMed Central for supplementary material.

ACKNOWLEDGMENTS

This research was supported by the National Institutes of Health Pathway to Independence Award 4R00GM129460 (K.M.D.), the Beckman Young Investigator Program (K.M.D.), and Emory University start-up funds (K.M.D.). Additional support was provided by the National Science Foundation (NSF) under Grant No. CHE-2155060

(Y.P.) and the NSF Graduate Research Fellowship Program under Grant No. 1937971 (K.A.I.). Any opinions, findings, and conclusions or recommendations expressed in this material are those of the author(s) and do not necessarily reflect the views of the National Science Foundation. This research used resources of the Advanced Photon Source, a U.S. Department of Energy (DOE) Office of Science User Facility operated by Argonne National Laboratory under Contract No. DE-AC02-06CH11357. Sector 20 is also supported by the Canadian Light Source and its funding partners, while BioCARS is also supported by the National Institute of General Medical Sciences of the National Institutes of Health under grant number P41 GM118217. We are grateful to Robert Henning, Vukica Srajer, and Irina Kosheleva at Sector 14, as well as Shelly Kelly and Chengjun Sun at Sector 20 of the Argonne National Laboratory for their assistance with data collection and experimental setup. We additionally thank Jamal Musaei and Alex Kaledin at Emory University's Cherry L. Emerson Center for Scientific Computation for assistance with DFT calculations.

REFERENCES

- (1). Chen AY; Adamek RN; Dick BL; Credille CV; Morrison CN; Cohen SM Targeting Metalloenzymes for Therapeutic Intervention. *Chem. Rev* 2019, 119, 1323–1455. [PubMed: 30192523]
- (2). Spilburg CA; Bethune JL; Vallee BL Kinetic Properties of Crystalline Enzymes. *Carboxypeptidase A. Biochemistry* 1977, 16, 1142–1150. [PubMed: 402935]
- (3). Doscher MS; Richards FM The Activity of an Enzyme in the Crystalline State: Ribonuclease S. *J. Biol. Chem* 1963, 238, 2399–2406.
- (4). Glatzel P; Bergmann U High Resolution 1s Core Hole X-ray Spectroscopy in 3d Transition Metal Complexes—Electronic and Structural Information. *Coord. Chem. Rev* 2005, 249, 65–95.
- (5). Kern J; Tran R; Alonso-Mori R; Koroidov S; Echols N; Hattne J; Ibrahim M; Gul S; Laksmono H; Sierra RG; et al. Taking Snapshots of Photosynthetic Water Oxidation Using Femtosecond X-ray Diffraction and Spectroscopy. *Nat. Commun* 2014, 5, 4371–4381. [PubMed: 25006873]
- (6). Kowalska J; DeBeer S The Role of X-ray Spectroscopy in Understanding the Geometric and Electronic Structure of Nitrogenase. *Biochim. Biophys. Acta* 2015, 1853, 1406–1415. [PubMed: 25486459]
- (7). Davis KM; Sullivan BT; Palenik MC; Yan L; Purohit V; Robison G; Kosheleva I; Henning RW; Seidler GT; Pushkar Y Rapid Evolution of the Photosystem II Electronic Structure During Water Splitting. *Phys. Rev. X* 2018, 8, 41014–41024.
- (8). Fransson T; Chatterjee R; Fuller FD; Gul S; Weninger C; Sokaras D; Kroll T; Alonso-Mori R; Bergmann U; Kern J; et al. X-ray Emission Spectroscopy as an In Situ Diagnostic Tool for X-ray Crystallography of Metalloproteins Using an X-ray Free-Electron Laser. *Biochemistry* 2018, 57, 4629–4637. [PubMed: 29906115]
- (9). Alonso-Mori R; Kern J; Gildea RJ; Sokaras D; Weng T-C; Lassalle-Kaiser B; Tran R; Hattne J; Laksmono H; Hellmich J; et al. Energy-Dispersive X-ray Emission Spectroscopy Using an X-ray Free-Electron Laser in a Shot-by-Shot Mode. *Proc. Natl. Acad. Sci* 2012, 109, 19103–19107. [PubMed: 23129631]
- (10). Bergmann U; Kern J; Schoenlein RW; Wernet P; Yachandra VK; Yano J Using X-ray Free-Electron Lasers for Spectroscopy of Molecular Catalysts and Metalloenzymes. *Nat. Rev. Phys* 2021, 3, 264–282. [PubMed: 34212130]
- (11). Fransson T; Alonso-Mori R; Chatterjee R; Cheah MH; Ibrahim M; Hussein R; Zhang M; Fuller F; Gul S; Kim IS; et al. Effects of X-ray Free-Electron Laser Pulse Intensity on the Mn K $\beta_{1,3}$ X-ray Emission Spectrum in Photosystem II - A Case Study for Metalloprotein Crystals and Solutions. *Struct. Dyn* 2021, 8, 64302–64315.
- (12). Jensen SC; Sullivan B; Hartzler DA; Aguilar JM; Awel S; Bajt S. a.; Basu S; Bean R; Chapman HN; Conrad C; et al. X-Ray Emission Spectroscopy at X-Ray Free Electron Lasers: Limits to Observation of the Classical Spectroscopic Response for Electronic Structure Analysis. *J. Phys. Chem. Lett* 2019, 10, 441–446. [PubMed: 30566358]
- (13). Blachucki W; Kayser Y; Czapla-Masztafiak J; Guo M; Juranic P; Kavcic M; Kallman E; Knopp G; Lundberg M; Milne C; et al. Inception of Electronic Damage of Matter by Photon-Driven Post-Ionization Mechanisms. *Struct. Dyn* 2019, 6, 24901–24908.

- (14). Davis KM; Kosheleva I; Henning RW; Seidler GT; Pushkar Y Kinetic Modeling of the X-ray-Induced Damage to a Metalloprotein. *J. Phys. Chem. B* 2013, 117, 9161–9169. [PubMed: 23815809]
- (15). Weik M; Ravelli RB; Kryger G; McSweeney S; Raves ML; Harel M; Gros P; Silman I; Kroon J; Sussman JL Specific Chemical and Structural Damage to Proteins Produced by Synchrotron Radiation. *Proc. Natl. Acad. Sci* 2000, 97, 623–628. [PubMed: 10639129]
- (16). de la Mora E; Coquelle N; Bury CS; Rosenthal M; Holton JM; Carmichael I; Garman EF; Burghammer M; Colletier J-P; Weik M Radiation Damage and Dose Limits in Serial Synchrotron Crystallography at Cryo- and Room Temperatures. *Proc. Natl. Acad. Sci* 2020, 117, 4142–4151. [PubMed: 32047034]
- (17). Pfanzagl V; Beale JH; Michlits H; Schmidt D; Gabler T; Obinger C; Djinovi -Carugo K; Hofbauer S X-ray-Induced Photoreduction of Heme Metal Centers Rapidly Induces Active-Site Perturbations in a Protein-Independent Manner. *J. Biol. Chem* 2020, 295, 13488–13501. [PubMed: 32723869]
- (18). Kryatov SV; Rybak-Akimova EV; Schindler S Kinetics and Mechanisms of Formation and Reactivity of Non-Heme Iron Oxygen Intermediates. *Chem. Rev* 2005, 105, 2175–2226. [PubMed: 15941212]
- (19). Huang X; Groves JT Oxygen Activation and Radical Transformations in Heme Proteins and Metalloporphyrins. *Chem. Rev* 2018, 118, 2491–2553. [PubMed: 29286645]
- (20). Bruice TC; Benkovic SJ Chemical Basis for Enzyme Catalysis. *Biochemistry* 2000, 39, 6267–6274. [PubMed: 10828939]
- (21). Pallotta MT; Rossini S; Suvieri C; Coletti A; Orabona C; Macchiarulo A; Volpi C; Grohmann U Indoleamine 2,3-Dioxygenase 1 (IDO1): an Up-to-Date Overview of an Eclectic Immunoregulatory Enzyme. *FEBS J* 2021, 289, 1–20.
- (22). Prendergast GC; Smith C; Thomas S; Mandik-Nayak L; Laury-Kleintop L; Metz R; Muller AJ Indoleamine 2,3-Dioxygenase Pathways of Pathogenic Inflammation and Immune Escape in Cancer. *Cancer Immunol. Immunother* 2014, 63, 721–735. [PubMed: 24711084]
- (23). Moon YW; Hajjar J; Hwu P; Naing A Targeting the Indoleamine 2,3-Dioxygenase Pathway in Cancer. *J. Immunother. Cancer* 2015, 3, 51. [PubMed: 26674411]
- (24). Moffett JR; Namboodiri MA Tryptophan and the Immune Response. *Immunol. Cell Biol* 2003, 81, 247–265. [PubMed: 12848846]
- (25). Jensen SC; Sullivan B; Hartzler DA; Pushkar Y DIY XES—Development of an Inexpensive, Versatile, and Easy to Fabricate XES Analyzer and Sample Delivery System. *X-Ray Spectrom* 2019, 48, 336–344.
- (26). Glatzel P; Bergmann U; de Groot FMF; Cramer SP Influence of the Core Hole on K β Emission Following Photoionization or Orbital Electron Capture: A Comparison using MnO and ⁵⁵Fe₂O₃. *Phys. Rev. B* 2001, 64, 45109–45119.
- (27). Peng G; deGroot FMF; Hámáláinen K; Moore JA; Wang X; Grush MM; Hastings JB; Siddons DP; Armstrong WH; Mullins OC; et al. High-Resolution Manganese X-ray Fluorescence Spectroscopy. Oxidation-State and Spin-State Sensitivity. *J. Am. Chem. Soc* 1994, 116, 2914–2920.
- (28). Lafuerza S; Carlantuono A; Retegan M; Glatzel P Chemical Sensitivity of K β and K α X-ray Emission from a Systematic Investigation of Iron Compounds. *Inorg. Chem* 2020, 59, 12518–12535. [PubMed: 32830953]
- (29). Gamblin SD; Urch DS Metal K β X-ray Emission Spectra of First Row Transition Metal Compounds. *J. Electron Spectros. Relat. Phenomena* 2001, 113, 179–192.
- (30). Castillo RG; Hahn AW; Van Kuiken BE; Henthorn JT; McGale J; DeBeer S Probing Physical Oxidation State by Resonant X-Ray Emission Spectroscopy: Applications to Iron Model Complexes and Nitrogenase. *Angew. Chem. Int. Ed* 2021, 60, 10112–10121.
- (31). Neese F Importance of Direct Spin–Spin Coupling and Spin-Flip Excitations for the Zero-Field Splittings of Transition Metal Complexes: A Case Study. *J. Am. Chem. Soc* 2006, 128, 10213–10222. [PubMed: 16881651]

- (32). Pollock CJ; Delgado-Jaime MU; Atanasov M; Neese F; DeBeer S $K\beta$ Mainline X-ray Emission Spectroscopy as an Experimental Probe of Metal–Ligand Covalency. *J. Am. Chem. Soc* 2014, 136, 9453–9463. [PubMed: 24914450]
- (33). Lee N; Petrenko T; Bergmann U; Neese F; DeBeer S Probing Valence Orbital Composition with Iron $K\beta$ X-ray Emission Spectroscopy. *J. Am. Chem. Soc* 2010, 132, 9715–9727. [PubMed: 20578760]
- (34). Gamblin SD; Urch DS Metal $K\beta$ X-ray Emission Spectra of First Row Transition Metal Compounds. *J. Electron Spectrosc* 2001, 113, 179–192.
- (35). Vankó G; Neisius T; Molnár G; Renz F; Kárpáti S; Shukla A; de Groot FMF Probing the 3d Spin Momentum with X-ray Emission Spectroscopy: The Case of Molecular-Spin Transitions. *J. Phys. Chem. B* 2006, 110, 11647–11653. [PubMed: 16800459]
- (36). Kennedy BJ; Brain G; Murray KS Chlorophthalocyanine Iron(III). $FePc(-2)Cl$. A Spin-Admixed ($S = 3/2 / S = 5/2$) System. *Inorganica Chim. Acta* 1984, 81, 29–31.
- (37). Kennedy BJ; Murray KS; Zwack PR; Homborg H; Kalz W Spin States in Iron(III) Phthalocyanines Studied by Mössbauer, Magnetic Susceptibility, and ESR Measurements. *Inorg. Chem* 1986, 25, 2539–2545.
- (38). Dale BW; Williams RJP; Johnson CE; Thorp TL $S = 1$ Spin State of Divalent Iron. I. Magnetic Properties of Phthalocyanine Iron (II). *J. Chem. Phys* 1968, 49, 3441–3444.
- (39). Evangelisti M; Bartolome J; de Jongh LJ; Filoti G Magnetic Properties of α -Iron(II) Phthalocyanine. *Phys. Rev. B* 2002, 66, 4410–4421.
- (40). Luo S; Xu K; Xiang S; Chen J; Chen C; Guo C; Tong Y; Tong L High-Resolution Structures of Inhibitor Complexes of Human Indoleamine 2,3-Dioxygenase 1 in a New Crystal Form. *Acta Crystallogr. F Struct. Biol. Commun* 2018, 74, 717–724. [PubMed: 30387777]
- (41). Davydov RM; Chauhan N; Thackray SJ; Anderson JLR; Papadopoulou ND; Mowat CG; Chapman SK; Raven EL; Hoffman BM Probing the Ternary Complexes of Indoleamine and Tryptophan 2,3-Dioxygenases by Cryoreduction EPR and ENDOR Spectroscopy. *J. Am. Chem. Soc* 2010, 132, 5494–5500. [PubMed: 20353179]
- (42). Papadopoulou ND; Mewies M; McLean KJ; Seward HE; Svistunenko DA; Munro AW; Raven EL Redox and Spectroscopic Properties of Human Indoleamine 2,3-Dioxygenase and a His303Ala Variant: Implications for Catalysis. *Biochemistry* 2005, 44, 14318–14328. [PubMed: 16245948]
- (43). Sugimoto H; Oda S; Otsuki T; Hino T; Yoshida T; Shiro Y Crystal Structure of Human Indoleamine 2,3-Dioxygenase: Catalytic Mechanism of O_2 Incorporation by a Heme-Containing Dioxygenase. *Proc. Natl. Acad. Sci* 2006, 103, 2611–2616. [PubMed: 16477023]
- (44). Terentis AC; Thomas SR; Takikawa O; Littlejohn TK; Truscott RJ; Armstrong RS; Yeh SR; Stocker R The Heme Environment of Recombinant Human Indoleamine 2,3-Dioxygenase. *J. Biol. Chem* 2002, 277, 15788–15794. [PubMed: 11867636]
- (45). Solovyev M; Kucheryavy P; Lockard JV Local Coordination and Electronic Structure Ramifications of Guest-Dependent Spin Crossover in a Metal-Organic Framework: A Combined X-ray Absorption and Emission Spectroscopy Study. *Inorg. Chem* 2022, 61, 9213–9223. [PubMed: 35678726]
- (46). Sono M; Taniguchi T; Watanabe Y; Hayaishi O Indoleamine 2,3-Dioxygenase: Equilibrium Studies of the Tryptophan Binding to the Ferric, Ferrous, and CO-Bound Enzymes. *J. Biol. Chem* 1980, 255, 1339–1345. [PubMed: 7354029]
- (47). Mirgaux M; Leherter L; Wouters J Influence of the Presence of the Heme Cofactor on the JK-Loop Structure in Indoleamine 2,3-Dioxygenase 1. *Acta Crystallogr. D Struct. Biol* 2020, 76, 1211–1221. [PubMed: 33263327]
- (48). Mirgaux M; Leherter L; Wouters J Temporary Intermediates of L-Trp Along the Reaction Pathway of Human Indoleamine 2,3-Dioxygenase 1 and Identification of an Exo Site. *Int. J. Tryptophan Res* 2021, 14, 1–11.
- (49). Yonetani T; Anni H Yeast Cytochrome c Peroxidase. Coordination and Spin States of Heme Prosthetic Group. *J. Biol. Chem* 1987, 262, 9547–9554. [PubMed: 3036864]

- (50). Khubbutdinov R; Menushenkov AP; Vartanyants IA Coherence Properties of the High-Energy Fourth-Generation X-ray Synchrotron Sources. *J. Synchrotron Radiat* 2019, 26, 1851–1862. [PubMed: 31721727]
- (51). Shin S New Era of Synchrotron Radiation: Fourth-Generation Storage Ring. *AAPPS Bulletin* 2021, 31, 1–16.
- (52). Neutze R; Wouts R; van der Spoel D; Weckert E; Hajdu J Potential for Biomolecular Imaging with Femtosecond X-ray Pulses. *Nature* 2000, 406, 752–757. [PubMed: 10963603]

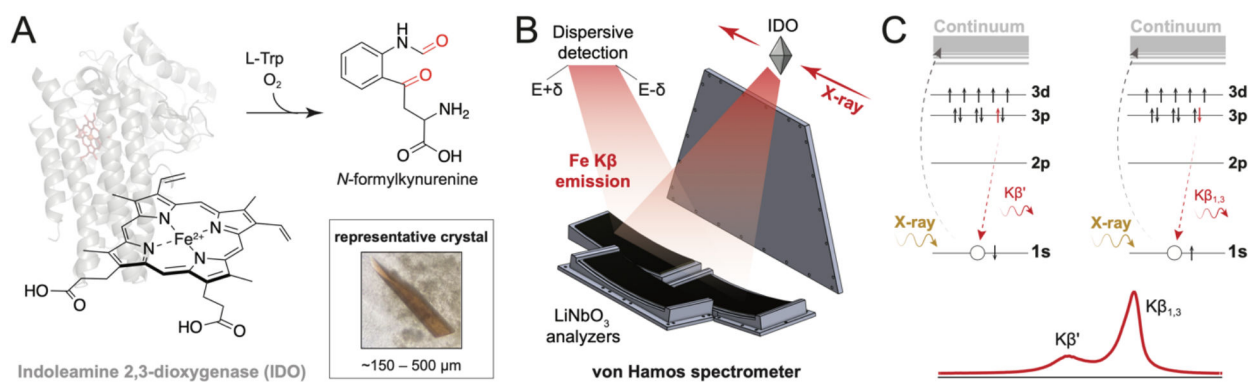


Figure 1. (A) IDO structure, reaction, and representative crystal used in this study. (B) Design schematic for Fe $K\beta$ von Hamos spectrometer. (C) Pictorial depiction of electronic transitions following excitation of a core electron that give rise to the $K\beta$ mainlines.

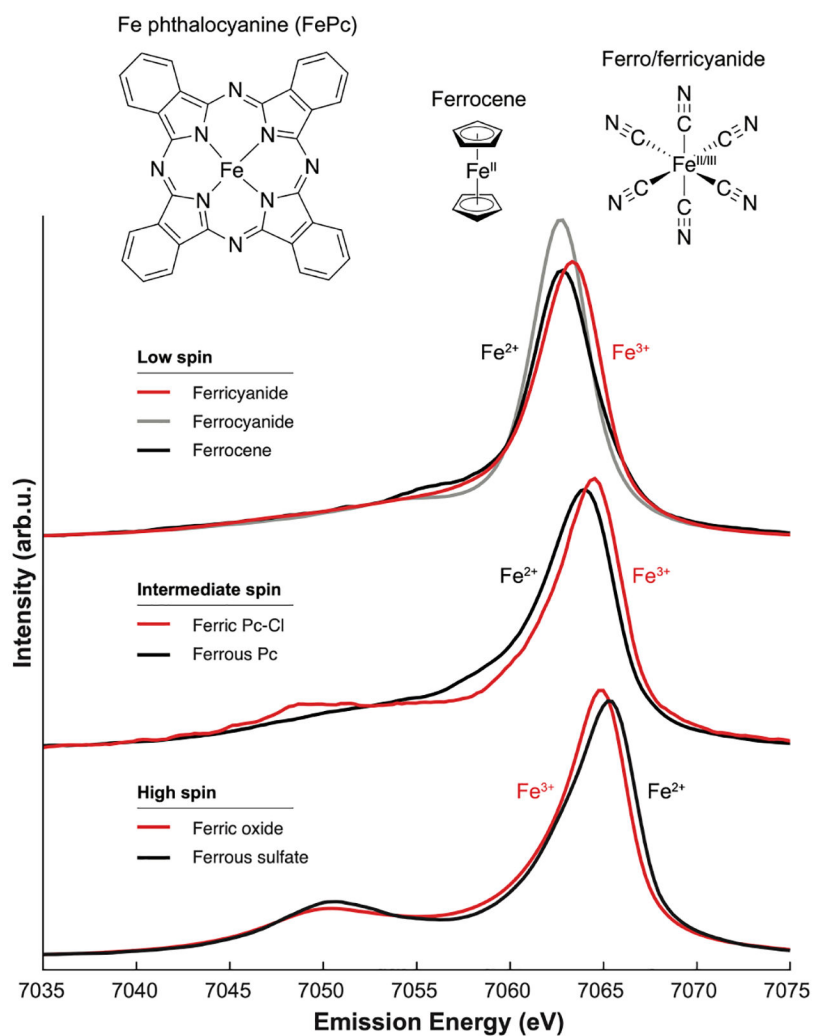


Figure 2. Emission spectra for a series of Fe standards demonstrate changes in peak position and shape due to oxidation and spin state. Spectra were normalized by the integral of the mainline peaks (see SI for more information).

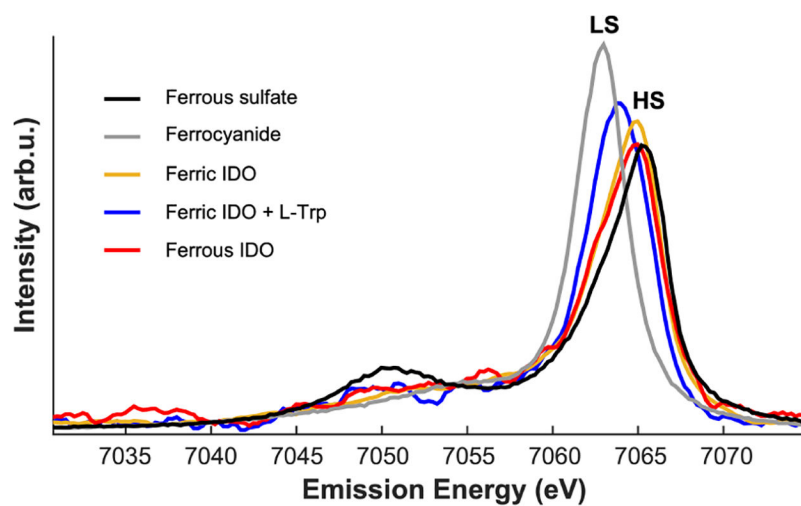


Figure 3. Emission spectra from single crystals of different IDO complexes compared to ferrous standards. Data were collected at 100 K.

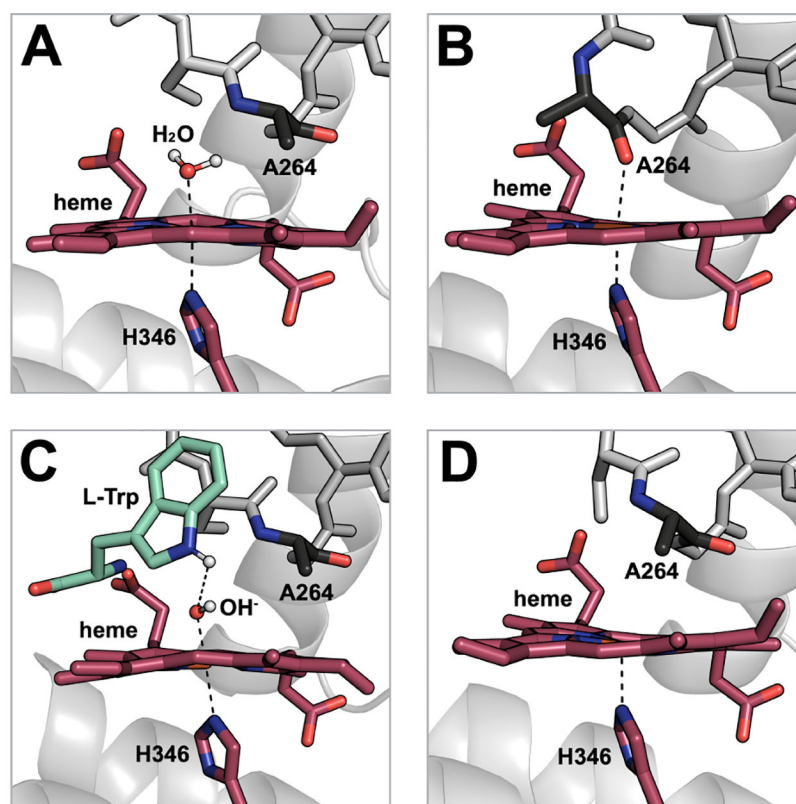
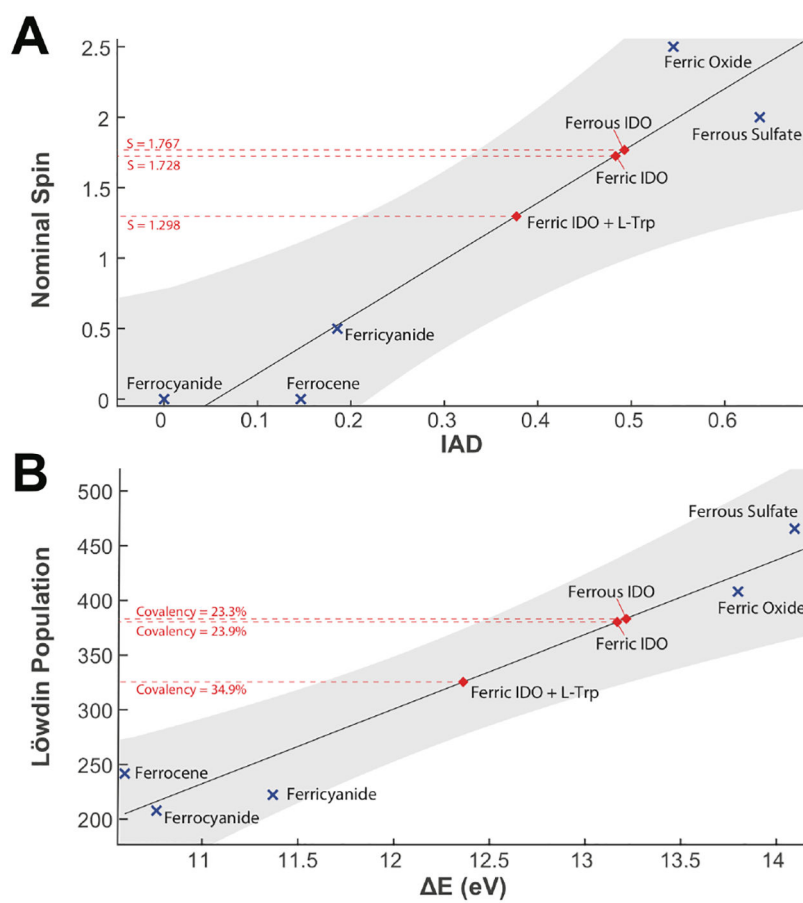


Figure 4. Active site configurations for various states of IDO. (A) Ferric IDO with water coordinated to the metal ion (PDB ID: 6E40). The water pictured was added *in silico* based on the DFT-optimized position (Table S13). (B) Ferric IDO with Ala264 coordinated to the metal ion (PDB ID: 6E44). (C) Ferric IDO with hydroxide coordinated to the metal ion and L-Trp bound in the active site (PDB ID: 6E35). Cyanide was removed from 6E35 and replaced by hydroxide in the DFT-optimized position for visualization (Table S11). (D) Five-coordinate ferrous IDO (PDB ID: 6E45).

**Figure 5.**

(A) IAD analysis based on a reference curve generated from a set of known spin state Fe standards (see Fig. S1). Grey shading indicates 95% confidence interval of fit. (B) Similar covalency analysis based on a comparison of $K\beta_{1,3}$ and $K\beta'$ peak splitting and DFT orbital population calculations.

Table 1.

Characteristics of Fe complexes from formal, spectral, and computational analysis.

Name	Spin State	Nominal Spin	Spin Density ^a	IAD	IAD-Spin	1 st Moment (eV)	Covalency ^b
Ferric oxide	HS	2.5	2.40	0.55	–	7064.56	18.4
Ferrous sulfate	HS	2	2.18	0.64	–	7064.83	7.0
Fe(III)Pc-Cl	mix	~1.85	1.69	0.49	1.75	7063.73	32.6
Fe(II)Pc	IS	~1	1.04	0.37	1.25	7064.25	33.7
Ferricyanide	LS	0.5	0.48	0.19	–	7063.30	55.6
Ferrocyanide	LS	0	0	0	–	7062.79	58.6
Ferrocene	LS	0	0	0.15	–	7062.99	51.6
Ferrous IDO	HS ^c	2 ^c	2.02	0.49	1.77	7064.34	23.3
Ferric IDO	mix	~1.5	1.54	0.48	1.73	7064.46	23.9
Ferric IDO + W	mix	~1.26	1.22	0.38	1.30	7063.88	34.9

^aDFT-derived spin densities, corrected using the fit in Fig. S2.^bPercent covalency for the Fe standards was determined via QRO methods, while IDO covalency values were predicted from the reference curve in Fig. S2.^cSpin state may differ at low temperatures. See SI for computational details and DFT coordinates (Fig. S3–S4 and Tables S2–S15).